Fabrication of 3D printed antimicrobial polycaprolactone scaffolds for tissue engineering applications

Socrates Radhakrishnan, Sakthivel Nagarajan, Habib Belaid, Cynthia Farha, Igor Iatsunskyi, Emerson Coy, Laurence Soussan, Vincent Huon, Jonathan Barés, Catherine Teyssier, et al.

Fabrication of 3D printed antimicrobial polycaprolactone scaffolds for tissue engineering applications

Socrates Radhakrishnan[1,2μ], Sakthivel Nagarajan[2μ], Habib Belaid[2,3], Cynthia Farha[2], Igor Iatsunskyi[4], Emerson Coy[4], Laurence Soussan[2], Vincent Huon[5], Jonathan Bares[5], Catherine Teyssier[3], Sébastien Balme[2], Philippe Miele[2,6], David Cornu[2], Narayana Kalkura[1], Vincent Cavaillès[3] and Mikhael Bechelany[2*]

1. Crystal Growth Centre, Anna University, Chennai, India, 600025.
2. Institut Européen des Membranes, IEM UMR 5635, Univ Montpellier, CNRS, ENSCM, Montpellier, France
3. IRCM, Institut de Recherche en Cancérologie de Montpellier, INSERM U1194, Université Montpellier, Montpellier F-34298, France
4. NanoBioMedical Centre, Adam Mickiewicz University, 3 Wszechnicy Piastowskiej str., 61-614, Poznan, Poland
5. LMGC, Laboratoire de Mécanique et Génie Civil, Université Montpellier, CNRS, Montpellier, France
6. Institut Universitaire de France (IUF), 1 rue Descartes, Paris F-73231, France

μ Authors contributed equally

*Corresponding author: mikhael.bechelany@umontpellier.fr, Phone: +33467149167, Fax: +33467149119

GRAPHICAL ABSTRACT

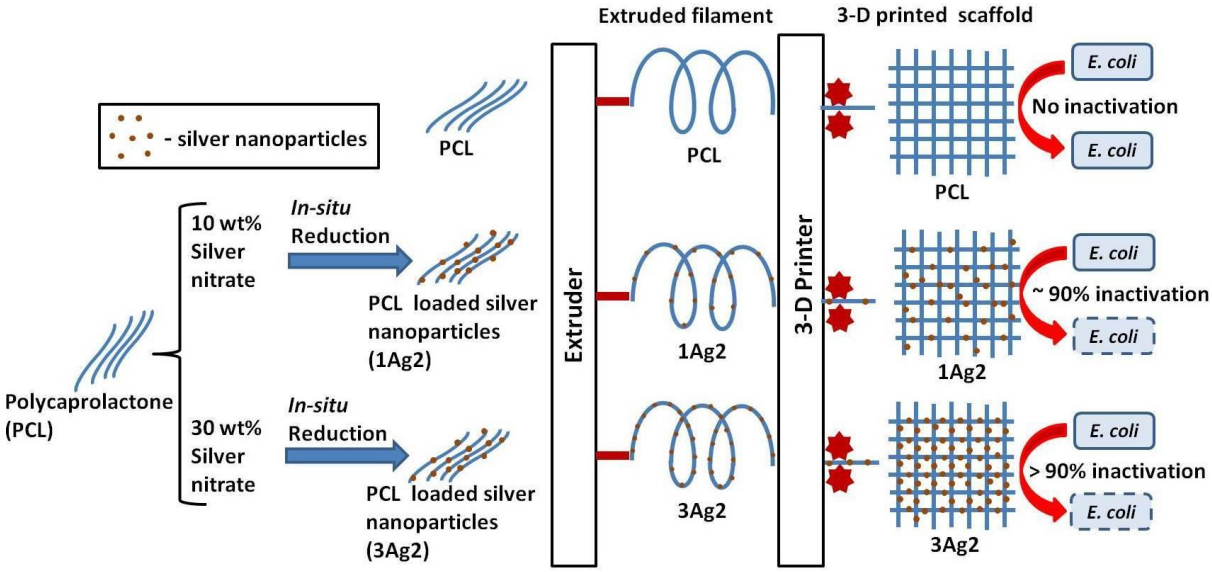

ABSTRACT

Synthetic polymers are widely employed for bone tissue engineering due to their tunable physical properties and biocompatibility. Inherently, most of these polymers display poor antimicrobial properties. Infection at the site of implantation is a major cause for failure or delay in bone healing process and the development of antimicrobial polymers is highly desired. In this study, silver nanoparticles (AgNps) were synthesized in polycaprolactone (PCL) solution by in-situ reduction which was further extruded into PCL/AgNp filaments. Customized 3D structures were then fabricated using the PCL/AgNp filaments through 3D printing technique. As demonstrated by scanning electron microscopy, the 3D printed scaffolds exhibited interconnected porous structures which are crucial for cell infiltration. Furthermore, X-ray photoelectron spectroscopy analysis revealed the reduction of silver ion. Transmission electron microscopy along with energy-dispersive X-ray spectroscopy analysis revealed the formation of silver nanoparticles throughout the PCL matrix. *In vitro* enzymatic degradation studies showed that the PCL/AgNps scaffolds displayed 80% degradation in 20 days. The scaffolds were cyto-compatible, as assessed by using MG63 cells and their antibacterial activity was demonstrated on *Escherichia coli*. Due to their interconnected porous structure, mechanical and antibacterial properties, these cyto-compatible multifunctional 3D printed PCL/AgNps scaffolds are highly suitable for bone tissue engineering.

Keywords:
polycaprolactone, silver nanoparticles, nanocomposites, cytocompatibility, antimicrobial, multifunctional properties

Highlights:

We report the development of antimicrobial polycaprolactone scaffold by 3D printing
The silver nanoparticles (AgNps) were obtained by in-situ reduction in PCL solution
AgNps reinforcement improved the stiffness of the 3D printed scaffolds
3D printed scaffold exhibited multifunctional property
Fabricated 3D scaffold showed cytocompatibility and antimicrobial properties

INTRODUCTION

Fused deposition modelling (FDM) is one of the simple and cost effective techniques employed in 3D printing of polymers for bone tissue engineering[1-2]. Various thermoplastic polymers such as poly-ε-capro-lactone (PCL)[3], poly(L-lactic acid) (PLLA)[4] and poly-vinyl-alcohol (PVA)[5], have been used in 3D printing. Among them, PCL was widely used for the fabrication of bone scaffolds because of its FDA (Food and Drug Administration) approval, biocompatibility and biodegradation properties[6]. The low melting point (60°C) of PCL is advantageous for 3D printing[7]. In addition, PCL exhibits good mechanical properties with high flexibility and great elongation at break[8], interesting for the preparation of scaffolds for craniofacial bone repair and cranial defects[9]. However, optimization of 3D printed PCL scaffolds by including other multifunctional properties such as antimicrobial activity and mechanical performance, without compromising their biocompatibility, is crucial to employ the scaffold for biomedical application.

About 2 to 5% of orthopaedic implants are complicated by infection[10] and this can raise up to 30% in the case of open fractures[11]. Implant related infections are associated with significant morbidity and sometimes death. These complications lead to implant removal, surgical debridement of infected tissue and long-term antibiotic administration[12-13]. Loading of antibiotics or metallic component is an issue to impart antibacterial property to the scaffolds. For instance, Visscher *et al.* developed 3D printed PCL scaffolds containing macro- and micro-pores (obtained using porogen) and coated with antibiotic (®Cefazoline). These scaffolds were active against *S. aureus*[14]. This design is very potential, however the

alarming levels of antibiotic resistance bacteria implies the necessity for developing potential alternate to this approach.

Silver, copper and zinc as metallic components are shown to exhibit antibacterial properties[15]. Among them, silver has been widely used in research and clinics as a broad spectrum antibacterial agent and apart from antibacterial application, silver nanoparticles-polymer composite has been used as catalytic agent[16], super capacitors[17], electromagnetic interference (EMI) shielding[18], fuel cells[19] etc., Mechanism of the antibacterial activity of silver nanoparticles (AgNps) is unclear. However, a recent investigation by Qing et *al.* provides possible explanations: (i) Anchoring of AgNps on bacterial membrane leads to membrane rupture and cellular content leakage that result in the bacterial cell death, (ii) Small size nanoparticles infiltrate the membrane and interact with the biomolecules which result in the dysfunction of bacterial cell, and (iii) AgNps are likely to catalyze O_2 reduction into reactive oxygen species (ROS) whose accumulation leads to down regulation of antioxidant enzyme expression, DNA damages and apoptosis[20].

Silver ions and its metallic nanoparticles can be directly incorporated into inorganic materials or mixed with synthetic and biopolymeric materials for the fabrication of antibacterial 3D printed structures[21 22]. For example, Muwaffak *et al.* developed 3D printed antimicrobial wound dressing material by incorporating ionic silver, copper and zinc oxide onto the PCL polymer. Silver and copper based PCL material displayed better bactericidal property than the zinc based material. However, this study is very limited and the influence of ionic silver on biocompatibility was not analyzed.[23] AgNps were mixed with other synthetic polymers such as polyetheretherketone (PEEK) and 3D printed using FDM technique. The obtained scaffolds showed good antimicrobial properties[24]. Silver incorporation in tricalcium phosphate (as inorganic matrix) based 3D printed scaffolds facilitated differentiation of mesenchymal stem cells into osteoblasts[25]. PCL scaffolds were also synthesized with impregnated or surface coated silver nanoparticles in order to increase antibacterial activity[26-28]. The scaffolds fabricated through solvent casting and electrospinning technique display poor control over the architecture and the uncontrollable pore size in comparison to the 3D printing approach.

In this work, silver ions were *in situ* reduced into silver nanoparticles and encapsulated into the PCL matrix. The PCL composite (PCL/AgNps) was thermally extruded into PCL/AgNps filaments used for the fabrication of customized scaffolds by the FDM technique. After validation of *in situ* reduction, the enzymatic degradation of the scaffolds

was elaborately analyzed. The antibacterial activity of the PCL and PCL/AgNps scaffolds was analyzed. Furthermore, scaffold cytocompatibility was evaluated using hFOB cells in order to assess their potential use for bone tissue engineering applications.

Materials and Methods

Materials

Polycaprolactone (PCL, Mw~ 50000 Da) pellets were obtained from polymorph (UK). N,N-Dimethylformamide (DMF; 99.8%; CAS number 68-12-2; Sigma), Tetrahydrofuran (THF; 99%; CAS number 109-99-9; Sigma), silver nitrate ($AgNO_3$; CAS number 7761-88-8, Sigma) , Lipase cepacia (40.7 units/mg, CAS number 9001-62-1; Sigma), MEMα (Minimum Essential Medium α) (A10490-01; Gibco), MTT (3-(4,5-Dimethylthiazol-2-yl)-2,5-Diphenyltetrazolium Bromide) (98%; CAS number 298- 93 -1), fetal bovine serum (FBS) (CVFSVF00-01; Eurobio), 1% (V/V), penicillin/streptomycin (15140-122; Gibco), 0.05% Trypsin-EDTA (25300-054; Gibco), Dimethyl sulfoxide (DMSO) (23486.297; BDH Prolab), ethanol (96% vol; CAS number 64-17-5), phosphate buffered saline (PBS, P44717; Sigma), Lysogeny broth (LB) Miller culture medium (L3522; Sigma), microbiologic agar (A1296-1KG; Sigma), Bacteriopeptone (211677-500g; BD Biosciences), Yeast extract (9112001; Biokar diagnostics), Sodium Chloride (NaCl; 99%; CAS number 7647-14-5; Sigma), Potassium dihydrogen phosphate (KH_2PO_4; CAS number 7778-77-0), di-Sodium hydrogen phosphate dodecahydrate ($Na_2HPO_4.12H_2O$; CAS number: 10039-32-4 ; Sigma) and agar (CAS number 9002-18-0; Sigma) were obtained and used without further purification. hFOB osteoblastic cell line obtained from ATCC was used for cytocompatibility analysis. Non-pathogenic Gram-negative *Escherichia coli* bacterium (K12 DSM 423, from DSMZ, Germany) was used for the antibacterial study.

Preparation of PCL/AgNps composite and extrusion of composite filaments

PCL solution (10% w/v) was prepared by dissolving it in solvent mixture (7:3 volume ratio of THF and DMF respectively) at 90°C. Silver nitrate with 2 different percentages (1% and 3% w/v) was added into the PCL solution and the temperature of the solution was maintained at 90°C. Resultant solution was refluxed for 3 hours to facilitate the reduction of silver nitrate into silver nanoparticles. Brown polymer suspension was obtained which are cooled and precipitated using 300 mL of ethanol and dried at room temperature. PCL/AgNp composites prepared using 1% and 3% silver nitrate are denoted as C1Ag2 and C3Ag2. PCL, C1Ag2 and C3Ag2 were extruded into filament by Noztek pro extruder at 120 °C.

Fabrication of 3D printed PCL/AgNp scaffold

PCL/AgNp scaffolds were fabricated using FDM technique. Scaffolds structure was customized using DesignSpark Mechanical® 2.0 software. The extruded filament was cast into 3D printed matrix by using FDM based 3D printer (PRUSA i3) and the settings are reported in the Table 1. Furthermore the scaffold made from the filaments of PCL, C1Ag2 and C3Ag2 are denoted as PCL, 1Ag2 and 3Ag2.

Table 1 Printer settings employed for printing PCL and PCL/AgNp scaffolds

Nozzle Diameter	0.4 mm
Extrusion width	0.45 mm
Layer height	0.05 mm
Fill density	25%
Fill pattern	Cubic
Extruder temperature	140°C
Bed Temperature	25°C
Speed of print moves	20-30 mm/s

Physical and chemical characterizations of the polymer and scaffolds

Surface morphology of the scaffold was observed using HITACHI S4800 scanning electron microscopy system and the samples were sputter-coated for 30s using platinum/palladium for SEM analysis. Here, Image J software was employed to calculate the mean filament diameter by taking average at 20 points and the pore size by taking average of 8 pores, which is denoted as mean ± standard deviation. The Fourier transform infrared (FTIR) spectrum of the scaffold was recorded in the frequency range of 4000 – 600 cm^{-1} by NEXUS instrument in an attenuated total reflection (ATR) mode. X-Ray diffraction (XRD) analysis was performed by PANalytica Xpert powder XRD system using Cu Kα radiation, 2θ range of 10−80°. X-ray photoelectron spectroscopy (XPS) analysis was performed using KRATOS- AXIS Ultra DLD model having monochromatic Al-K alpha source of 1486.6 eV spectral resolution FWHM 0.45 eV. *In situ* synthesis of silver nanoparticles in the PCL polymer was characterized using TEM (JEOL ARM 200F) combined with an EDX Analyzer.

For TEM analysis, polymer samples were cut into 90 nm thick slices after fixing it in Devcon 5@Minute Epoxy using ultra microtome and mounted over the Cu grid. Mechanical properties of the PCL composites were assessed using a traction machine (MTS 1/ME) equipped with a 5 kN force sensor. PCL composites were 3D printed as standard dog bones shapes to measure the mechanical properties and the analysis was performed in the strain rate of 0.01 mm s^{-1}. Furthermore, Young's modulus and Poisson's ratio were calculated on minimum three assays as demonstrated elsewhere[29-30].

Enzymatic degradation of the PCL and PCL/AgNp scaffolds

In vitro degradation of the scaffolds was carried out using lipase enzyme at concentration of 10 units/mL. The lipase solution was prepared from 0.01 M phosphate-buffered saline (PBS) at pH 7.4. The samples were weighed and placed in a vial containing the 1 ml lipase solution and incubated at 37°C. Every 3 days, the enzyme solution was replenished with fresh lipase solution. After definite time, the samples were removed from the enzyme solution, washed, dried at 37°C and weighed. The percentage of degradation of the scaffold was calculated by measuring the ratio of the final weight of the sample to that of the initial weight (taken in the range of 9.0-15.0 mg) of the sample that is after and before the degradation.

Cell viability assay

hFOB osteoblastic cells were cultured using DMEM/F12 (Dulbecco's Modified Eagle Medium α) (Gibco 10565018) conditioned media supplemented with (i) 10 % (V/V) fetal bovine serum (FBS) (Eurobio CVFSVF00-01). Cells were cultured at 37°C in 5% CO_2 in a 10 cm diameter petri dish and trypsinized using 0.05% Trypsin-EDTA (Gibco 25300-054). After sterilization with 70% (w/v) ethanol for 30 mins, the printed scaffolds were dried at room temperature and then placed in contact with hFIB cells for 8 days. Cell viability was analyzed using MTT assay carried out by incubating 100 µL of 0.5 mg/mL of MTT solution on the cells for 3h. Purple coloured formazan crystals were dissolved using 40 µL of DMSO (BDH Prolab 23486.297) and the absorbance was recorded at 560 nm using Multiskan plate reader (thermos, USA).

Antibacterial activity

Antibacterial activity of the 3D PCL/AgNp scaffold was characterized by soft agar and liquid tests to study bacterial growth inhibition and bactericidal action respectively (the

detailed protocols are given in the supportive information S1). The samples used for the antibacterial activity trials were sterilized by immersion in a water/ethanol (3:7 *v/v*) solution for 1 h and washed afterwards for several times with sterile deionized water to remove the ethanol traces in the sample. Later the washed samples were sterilely dried at 30°C overnight and used for the antibacterial activity tests. Bacterial growth inhibition tests were carried out by putting the samples in contact with a nutritive soft agar inoculated with bacteria. Bactericidal action of the material was characterized by incubating the material in a suspension of resting bacteria (i.e., un-growing bacteria).

RESULTS AND DISCUSSION

PCL/AgNps composite was synthesized through in situ reduction –mechanism (equation 1 and 2) as described by Santos et al. [31]. Obtained PCL/AgNp was utilized for the fabrication of customized 3D printed structure (Figure 1). Physicochemical properties, biocompatibility as well as antimicrobial properties of the PCL and PCL/AgNps scaffolds were analyzed and discussed.

$$HCONMe_2 + 2Ag^+ + H_2O \longrightarrow 2Ag^0 + Me_2NCOOH + 2H^+ \quad (1)$$

Santos et al.[31]. described that the carbamic acid undergoes decomposition at high temperature followed by evaporation.

$$Me_2NCOOH \longrightarrow CO_2 + Me_2NH \quad (2)$$

Figure 1. Photograph of the 3D printed scaffolds (scale bar denotes 1cm)

Physicochemical properties of the scaffolds

Scanning electron microscopy SEM images of the 3D printed PCL and PCL/AgNps scaffolds are shown in the Figure 2. SEM micrographs revealed that the PCL and PCL/AgNps 3D scaffolds matrix displayed uniform porous structures with open and interconnected pores. Inter filament spacing resulting from the fusion of multiple layers of polymer filaments are denoted as pores as mentioned in the literature[21, 32]. 3D structure and pore size of the

scaffolds plays a crucial role in cell infiltration. Murphy *et al.* demonstrated that the scaffolds having 80 to 190 µm pore size display cell aggregation and poor cells infiltration. Scaffolds of 300 µm pores size possess improved cells infiltration and the cells were observed at the center of the scaffolds without cell aggregation. These results prove that the pores sizes above 300 µm is crucial in the scaffolds design[33]. Scaffolds obtained in our study displayed pore size larger than 300 µm (Table 2), this dimension being suitable for osteoblast cell infiltration. The diameter of 3D printed filaments is also shown in Table 2. SEM micrographs of 1Ag2 and 3Ag2 revealed homogeneous filament diameters which is crucial in order to obtain scaffolds with uniform architectures. High magnification SEM micrograph reveals wrinkly surface morphology for PCL and almost smooth and uniform surface for 1Ag2 and 3Ag2 (Figure 1). Here, AgNps act as the inorganic filler leading to the increased stiffness which is evident from the increased Young's modulus.

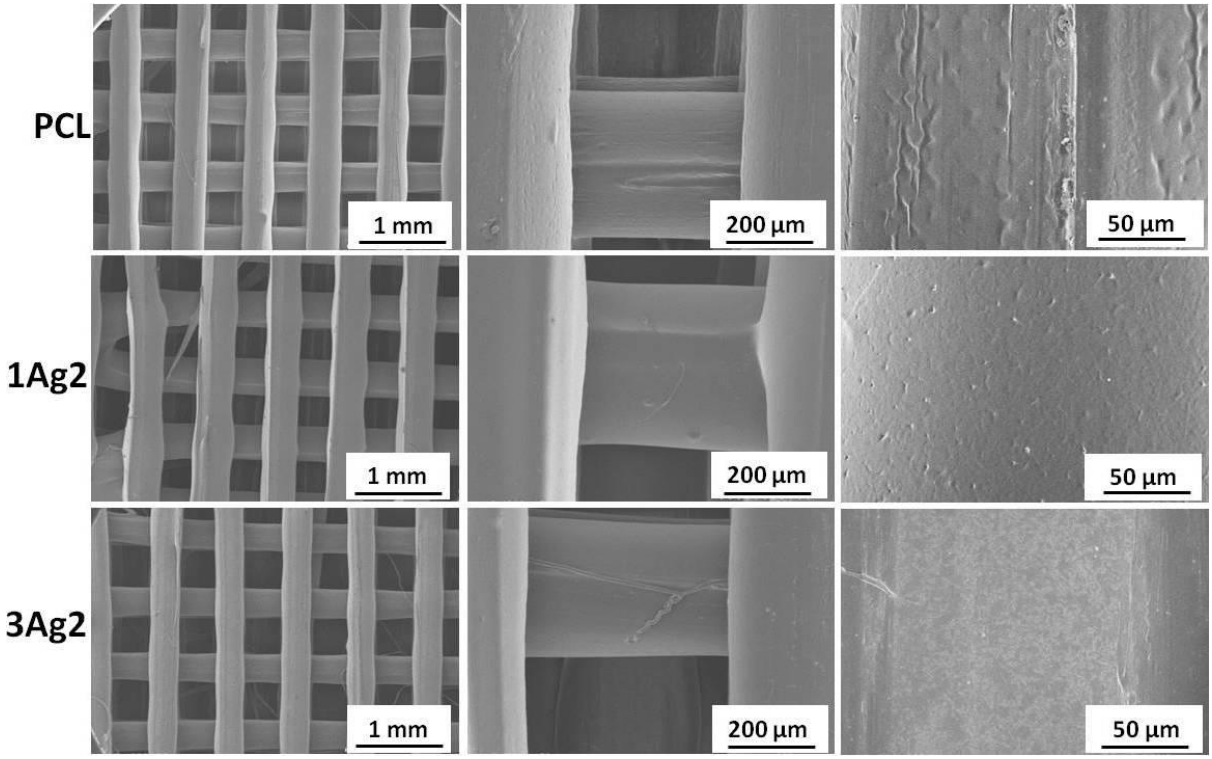

Figure 2. SEM analysis of 3D printed scaffolds

Table 2. Dimensions of the printed 3D scaffold

	PCL	1Ag2	3Ag2
Pore size (µm)	430.0 ± 29.8	379.6 ± 21.2	431.7 ± 24.6
Filament diameter (µm)	349.1 ± 21.6	406.4 ± 23.3	333.9 ± 12.0

FTIR analysis was used to identify the functional groups of the 3D printed PCL and PCL/AgNps scaffolds and the interaction between PCL and AgNps. The FTIR spectra are shown in Figure 3(A). The intense peak at 1721 cm^{-1} is assigned to the stretching mode of carbonyl groups of PCL. The peaks at 2865 cm^{-1} and 2944 cm^{-1} correspond to the symmetric and asymmetric stretching of CH_2 groups in PCL polymer backbone. The peaks at 1238 cm^{-1} and 1161 cm^{-1} are due to symmetric and asymmetric stretching of C-O-C groups of PCL. The peaks at 1187 cm^{-1} and 1292 cm^{-1} are related to O-C-O stretching, and C-O and C-C stretching modes respectively[34]. PCL display polar functional groups > C=O and –C-O-C- and their position of the corresponding peaks remains unaffected during the *in situ* reduction of silver ions into silver nanoparticles using DMF[35].

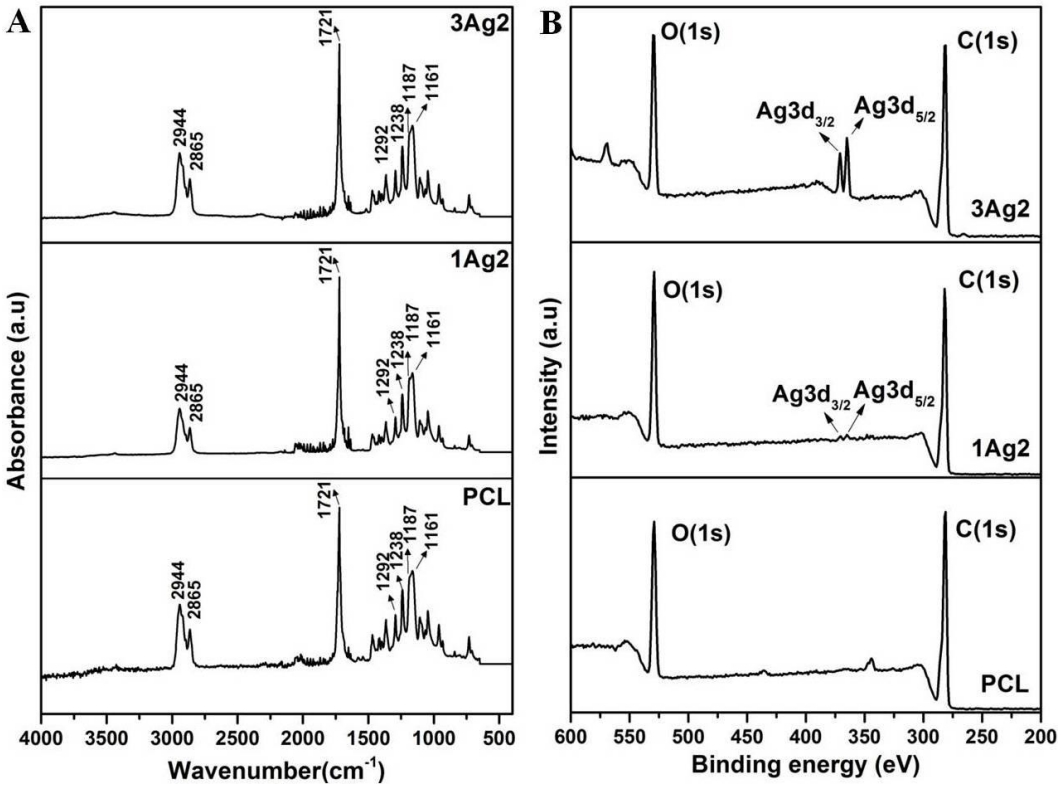

Figure 3. (A) FTIR and (B) XPS spectra of 3D printed scaffolds

X-ray photoelectron spectroscopy (XPS) analysis was used to confirm the formation of silver nanoparticles in the PCL/AgNp composite. The 3D printed scaffolds were scanned in the range of 200 to 600 eV.(figure 3(B)) The XPS spectra showed the peaks of C 1S, and O 1S which correspond to the PCL. The Ag 3d peaks ($3d_{3/2}$, $3d_{5/2}$) are observed in the 1Ag2 and

3Ag2 samples. They confirm the presence of silver in these scaffolds. The peak separation (energy difference of Ag3d peaks) of Ag $3d_{3/2}$, $3d_{5/2}$ is 6eV which corresponds to the reduced silver. These results show that the reduction of ionic silver into metallic silver is effectively achieved using DMF[31, 36-38]. Furthermore, silver concentration in 1Ag2 and 3Ag2 was quantified using AAS as 1.34 and 15.22 mg/g of the 3D printed matrix respectively.

X-ray diffraction (XRD) was used to determine the crystalline structures of the AgNps/PCL 3D printed scaffolds (Figure 4(A)) The XRD diffractogram of the scaffolds PCL, 1Ag2 and 3Ag2 are characterized by diffraction peaks at 2Θ = 21.2°, 21.7° and 23.5° which correspond to (110), (111) and (200) crystal planes of PCL respectively[39]. The diffraction peak observed at 38.8° (Figure 4(B)) in 1Ag2 and 3Ag2 diffractograms corresponds to the (111) plane of Ag. It confirms the presence of silver in 1Ag2 and 3Ag2 scaffolds.

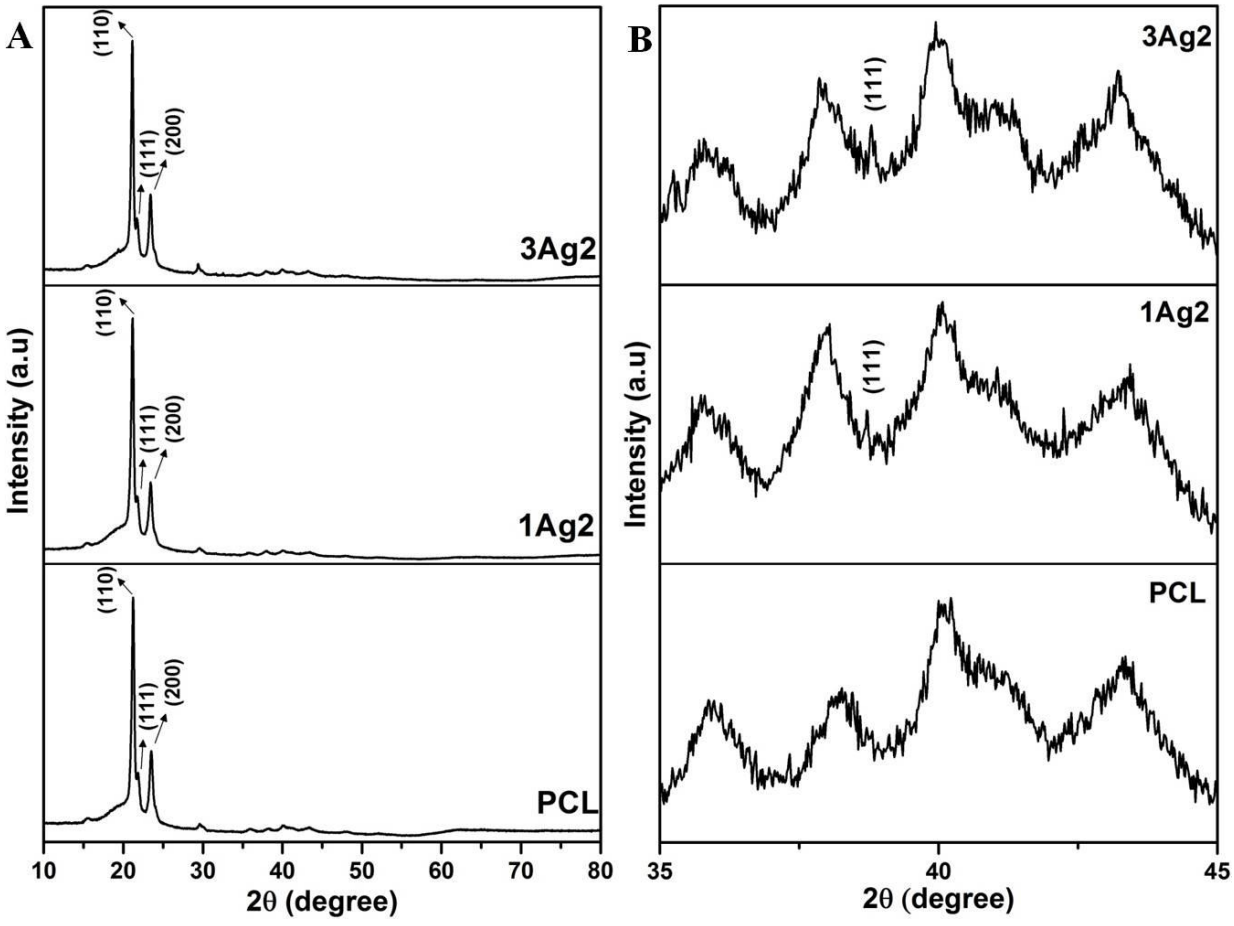

Figure 4. XRD analysis of 3D printed scaffolds, (A) Whole diffractogram and (B) diffractogram of specific regions.

In situ synthesis and distribution of the silver nanoparticles in the 3D printed PCL matrix was analyzed using transmission electron microscopy (TEM) along with EDX analysis (Figure 5(a-d)). TEM bright field micrographs of 3Ag2 clearly reveal the distribution of silver nanoparticles as spots throughout the PCL matrix (Figure 5(a, b)). The sizes distribution is in the range of 20 to 150 nm (Figure 5c) exemplifying wide dispersity of the synthesized silver nanoparticles. Furthermore, EDX analysis confirms the distribution of silver nanoparticles in the PCL polymer matrix. Therefore, the presence of the silver nanoparticles in the PCL matrix is probably responsible of the antibacterial activity as it will be demonstrated later.

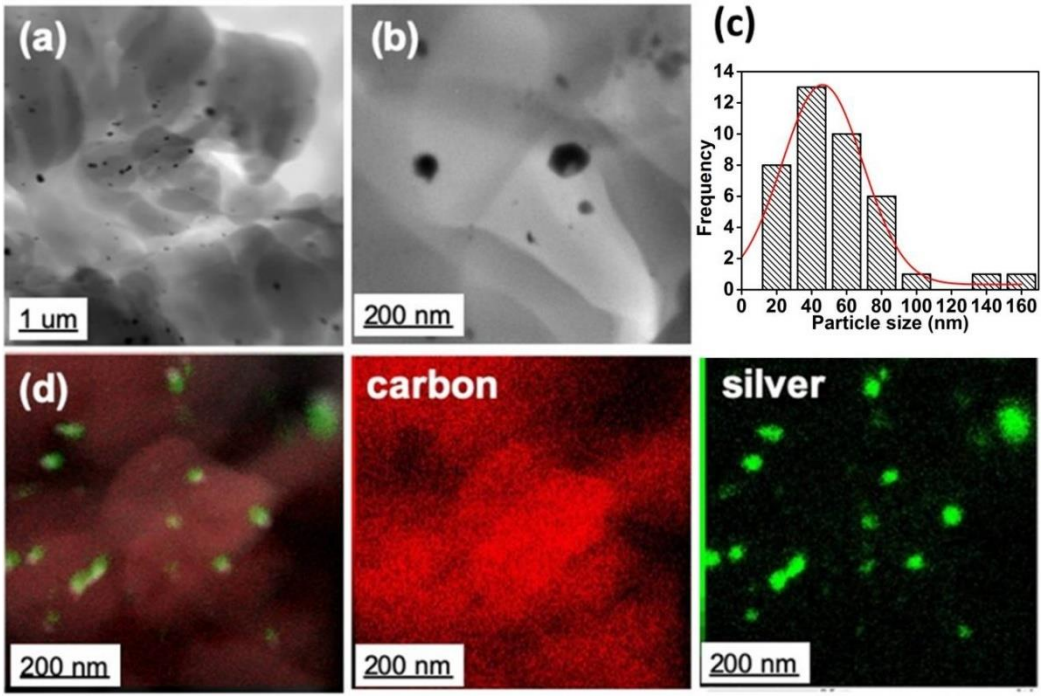

Figure 5. (a)-(b) TEM images of 3Ag2 sample, (c) Ag particle size distribution and (d) EDX elemental mapping of 3Ag2 scaffolds; Silver (green) and Carbon(red).

Materials used for implant tissue engineering applications should possess mechanical properties suitable for the targeted tissue. Therefore, the mechanical properties of 3D printed pristine PCL and PCL/Ag were characterized using tensile test analysis (Figure 6). Firstly the Poisson's ratio for PCL was 0.38 and remains constant with the addition of silver nanoparticles. Young's modulus of PCL was found to be 0.35 GPa which is in good agreement with the literature[40]. For PCL/Ag (1Ag2 and 3Ag2), the Young's modulus increases from 0.35 (PCL) to 1 GPa (3Ag2). Generally, the fillers restrict the mobility of polymer matrix and enhance the rigidity of the scaffolds[41-42]. In this study, silver nanoparticles are also acting as fillers which decrease the elastic behavior of PCL and

improve its rigidity. Furthermore, increasing the silver concentration enhanced the Young's modulus of the PCL/AgNP (1Ag1 and 3Ag2) composite scaffolds. Here, the values of Young's modulus of the composites are between that of the cancellous bone (0.05-0.1 GPa) and cortical bone (3-30 GPa)[43]. These results also support the employment of the composite scaffolds for bone tissue engineering application.

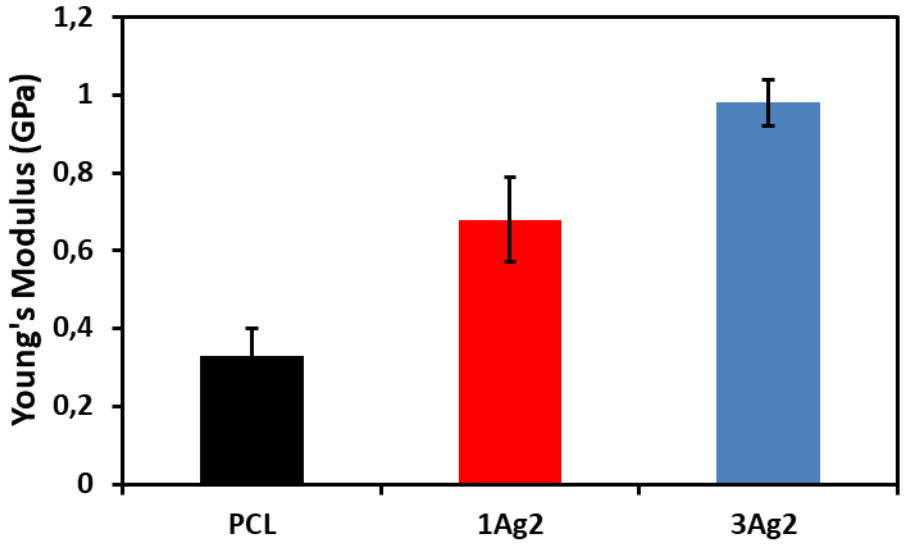

Figure 6. Mechanical property, Young's modulus of 3D printed scaffolds.

Enzymatic degradation test

In vitro enzymatic degradation analysis was used to evaluate stability of the 3D printed PCL/AgNp scaffolds. Lipase was employed because PCL possesses an ester bond prone to hydrolytic degradation by lipase. For this assay, the pre-weighed PCL, 1Ag2 and 3Ag2 scaffolds were immersed in the lipase solution and their degradation was recorded (Figure 6). PCL, 1Ag2 and 3Ag2 scaffolds display <10% degradation in 24 hours. The degradation of PCL scaffolds gradually increased to reach 82% degradation after 20 days. Generally, polymer undergoes surface degradation due to the direct contact of enzyme[44]. Scaffolds (PCL, 1Ag2 and 3Ag2) fabricated in this study are interconnected porous scaffolds which display large surface area to interact with enzymes that can facilitate the degradation. Neumann *et al*. 3D printed PCL and PCL/$CaCO_3$ scaffolds and analyzed the degradation of the scaffolds using 15U/mL lipase. Our material exhibits a degradation profile similar to the degradation profile obtained by Neumann *et al*. in which PCL undergoes 80% degradation in 20 days[45].

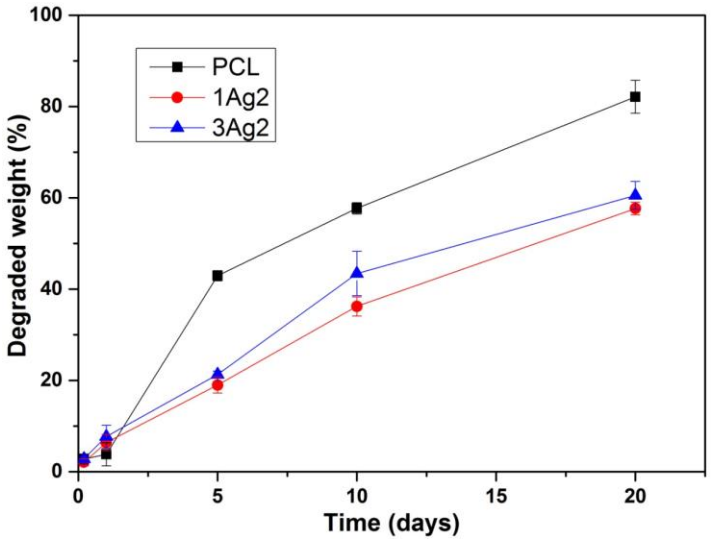

Figure 7. Enzymatic degradation of 3D printed scaffolds

Biocompatibility analysis

Biocompatibility of the PCL, 1Ag2 and 3Ag2 scaffolds was assessed using hFOB cells which are a good *in vitro* model of bone cells (REF?). Cells grown on the tissue culture plate without scaffold served as tissue culture plate control (TCP). Biocompatibility of the 3D printed scaffolds was calculated by comparing cell viability of the 3D printed scaffolds with the TCP control. Cell viability data shown in Figure 8 were presented as mean ± standard deviation (S.D) and statistical analysis done using Student's t test indicating "ns" not significant and * $p < 0.05$ with sample size, n=8.

Afer 8 days of culture, PCL scaffolds did not show any toxicity to the cells which evidences that the solvents employed for the preparation of 3D scaffolds are effectively removed. 1Ag2 allowed a better proliferation of the cells compared than PCL while 3Ag2 display a decrease in cell viability. Cell viability of 3Ag2 observed is likely due to the high concentration of silver loaded in the PCL matrix. However, cell viability was found to be greater than 80 % after 8 days which fits within the acceptable limits as set by ISO10993-5:2009. Despite their toxicity, silver and silver based formulation are utilized for commercial biomedical products such as PolyMem® Silver, Aquacel® Ag, Acticoat™, Urgotul®SSD, Contreet®. Indeed, silver can be eliminated through urinary excretion in humans[47]. Nevertheless, 3D printed PCL/AgNps display low cytotoxicity, suggesting that they could be suitable for tissue engineering application.

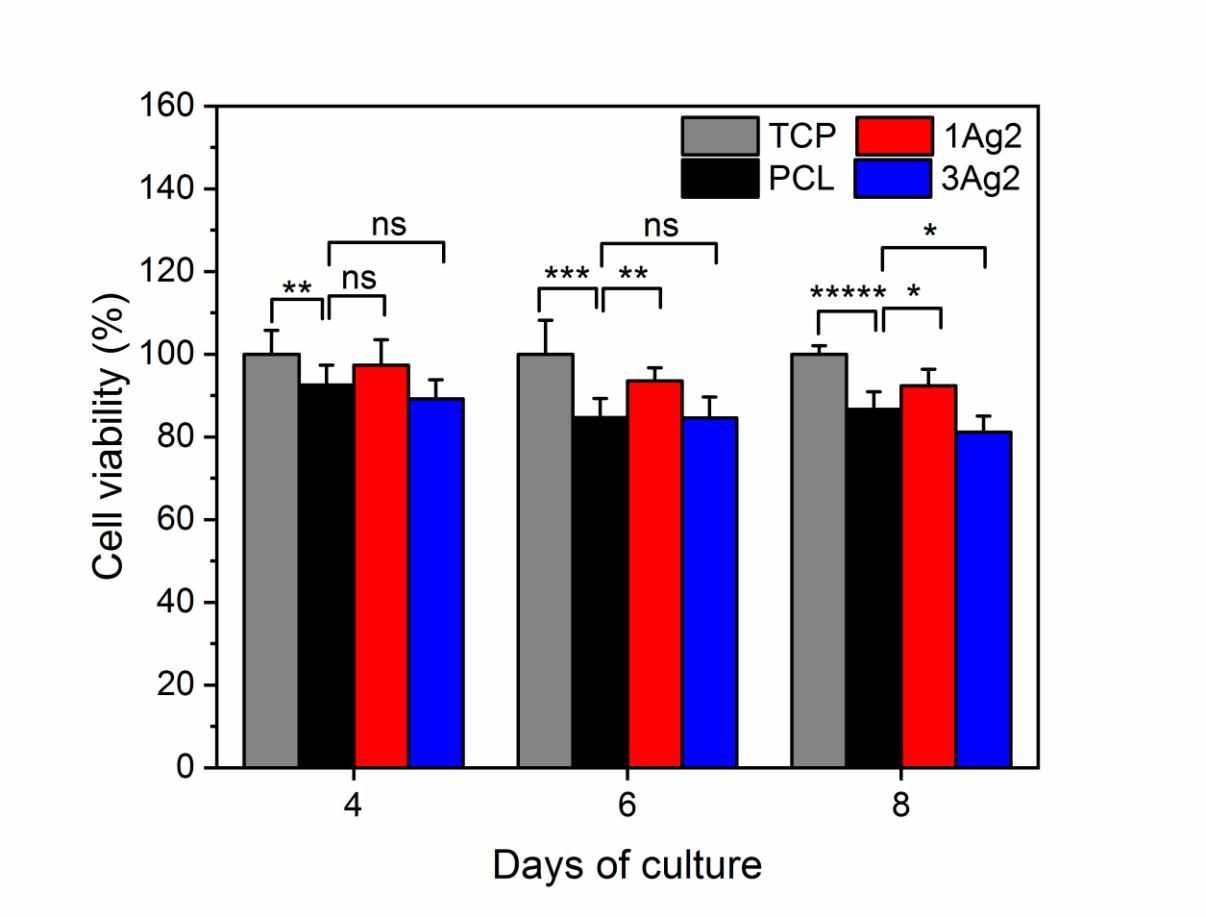

Figure 8. hFOB osteoblastic cell viability after 8 day of culture on of 3D printed scaffolds. (ns= not significant, * $p<0.05$, ** $p<0.005$ and ***** $p<0.000005$)

Bacterial growth inhibition test

Antibacterial activity of the materials was first characterized by growth inhibition tests. Bacterial growth inhibition test was performed to assess the ability of the material to prevent the implanted site from the formation of bacterial biofilm in presence of nutrients since it could lead to bacterial infection. Figure 9 presents the results obtained for the inhibition tests performed at 24 h.

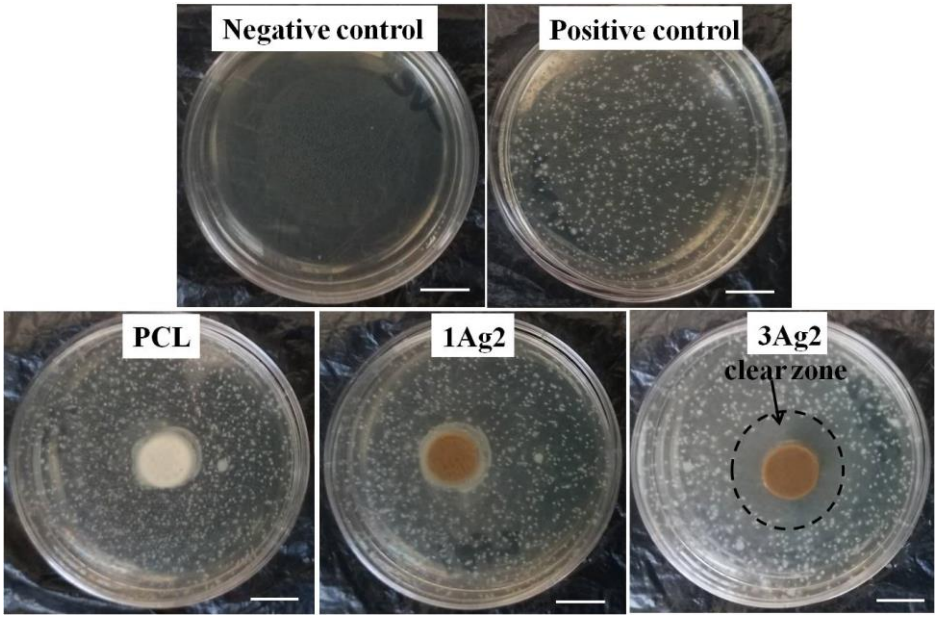

Figure 9. Soft agar plates inoculated with *E. coli* cells and incubated with 3D printed scaffolds in their center for 24 h (Scale bar denotes 1 cm)

Negative control plates (i.e. without bacteria and material) show clear nutritive soft agar plates while positive control plates (i.e., with bacteria and without material) show a uniform distribution of bacterial colonies within the soft agar (Fig. 9). With 3Ag2 material, a clear inhibition zone of mean diameter 20.4 ± 1.7 mm is observed whereas no clear zone is observed for PCL and 1Ag2 (Fig. 9) for which biofilms are evidenced on the material surfaces. The presence of an inhibition zone around the 3Ag2 material evidences an antibacterial activity based on the diffusion of biocidal agents through the soft agar. These biocidal agents might be silver (most likely Ag0 rather than Ag^+ according to XPS analysis) and/or ROS. This antibacterial activity does not exclude a bactericidal surface action by the AgNP present on the material, but the soft agar test does not allow to conclude on that.

Bactericidal activity

Bactericidal tests were done to assess the ability of the material to remove bacteria that has already grown on the material implantation zone. Bactericidal activity was assessed by liquid tests in which the material (90 ± 10 mg) was immersed in a bacterial suspension (10 mL) at about 10^2 CFU/mL. Table 3 shows the bacterial concentrations (CFU/mL) and the associated log-removal values, where the log-removal is defined as the logarithm (log) ratio of the bacterial concentration C measured after respective contact time relative to the initial bacterial concentration C_0. A log-removal value of -log (C_0) was attributed to the particular

case of total removal of the cultivable bacteria. A log-removal value higher than 1 is related to a significant bactericidal activity, i.e., to a reduction in bacterial concentration higher than 90 %. Table 3 reports also the total silver concentration measured by AAS in the liquid after 24 h contact.

Table 3. Log-removals and concentrations of released silver obtained in bactericidal tests against an *E. coli* suspension; the initial bacterial concentration C_0 was 175 ± 50 CFU/mL

	After 6 h contact		**After 24 h contact**		
Test	**Bacterial concentration (CFU/mL)**	**Log removal (-)**	**Bacterial concentration (CFU/mL)**	**Log removal (-)**	**Total silver concentration (mg/L)**
$C_{Positive\ control}$	**175 ± 50**	**0**	**175 ± 50**	**0**	**-**
C_{PCL}	115 ± 5	0.2	135 ± **0**	0.1	-
C_{1Ag2}	145 ± 40	0.1	10 ± 10	1.2	0.06
C_{3Ag2}	5 ± 5	1.5	0 ± **0**	2.2	0.44

PCL material shows a low log-removal value of 0.2 and 0.1 for 6 h and 24 h contact time respectively (Table 3). As PCL was not reported to have any antibacterial activity, the log-removal observed is probably due to bacteria adsorption on the PCL. It is thus likely that such an adsorption also occurred for the silver materials. After 6 h only, 3Ag2 material shows a significant decrease of the bacterial concentration corresponding to a log-removal value of 1.5 (Table 3), which is close to the maximal log-removal value reachable (i.e. $-\log C_0 = 2.2$). Hereafter 24 h, 1Ag2 depicted a marked decrease of bacterial concentration leading to a log-removal value of 1.2 and 3Ag2 material managed to inactivate all the bacteria initially present. This result clearly evidences the bactericidal activity of the 1Ag2 and 3Ag2 materials due to the presence of AgNPs in the material.

AAS measurements reveal that small silver concentrations were released in the suspension after 24 h (Table 3), which corresponds to silver mass lost by the material of 6.0×10^{-4} mg for 1Ag2 and 4.4×10^{-3} for 3Ag2 respectively. Since the initial silver content of the materials were 0.13 % *w/w* for 1Ag2 and 1.5 % *w/w* for 3Ag2, and the samples weight were 90 ± 10 mg, it means that the mass of silver incorporated in PCL were 0.12 mg for

1Ag2 and 1.35 mg for 3Ag2 respectively. After 24 h of reaction, 1Ag2 consequently lost 0.05 % of its silver whereas 3Ag2 lost 0.3 %. This result demonstrates the good chemical stability of both PCL/AgNps materials in presence of bacteria. In the case of 1Ag2, a bactericidal action of the surfaces is mainly evidenced because the silver released in the bacterial suspension is very small (< 0.1 mg/L). For 3Ag2, a coupled action of both the AgNps surface and the silver desorbed can be suspected. The need for a longer contact time (24 h vs 6 h) to observe a bactericidal activity of 1Ag2 might consequently be due to a lower content of silver nanoparticles on the material surface contacting the bacteria. These results are consistent with the fact that the antibacterial activity depends on the quantity of silver nanoparticles which is acting as the antibacterial agent[48].

Conclusion

PCL/AgNps polymer composite was achieved through *in situ* reduction of silver ions using DMF as a reducing agent as well as solvent. Synthesized PCL/AgNps composites were extruded into self-standing filaments further utilized for the fabrication of customized 3D porous structures using 3D printing technique. XRD, XPS, TEM and EDAX analysis confirmed the presence of silver nanoparticles within the 3D printed matrix. SEM analysis of the scaffolds shows that the 3D printed scaffolds displayed interconnected porous structures wrinkly surface on PCL and uniform smooth surface on 1Ag2 and 3Ag2 scaffolds. Here the presence of silver nanoparticles in the PCL scaffold improved its stiffness (Young's modulus) and enzymatic stability. Soft agar test showed that 3Ag2 scaffold exhibited an inhibition zone where *E. coli* growth is prevented around the scaffold due presumably to ROS and silver nanoparticles diffusion from PCL scaffold to soft agar. Besides, a biocidal surface action was evidenced for both 1Ag2 and 3Ag2. Furthermore, we show that the 3D printed scaffolds exhibit cytocompatibility. Altogether, our study shows that the scaffolds developed could be utilized for the fabrication of antimicrobial scaffolds for bone tissue engineering application.

Acknowledgements

The authors would like to thank for the financial support from Indo-French Centre for the promotion of advanced research-Cefipra (Project 5608-1). This study was supported as well by the University of Montpellier (MUSE "3DTraitCancer" project). I.I and E.C. acknowledge the partial financial support by project H2020-MSCA-RISE-2017, 'Novel 1D photonic metal oxide nanostructures for early stage cancer detection' (Project number: 778157). I.I. also acknowledges the support of dr. Łucja Przysiecka in TEM sample preparation.

References:

1. Gibson, I.; Rosen, D.; Stucker, B., The Impact of Low-Cost AM Systems. In *Additive Manufacturing Technologies: 3D Printing, Rapid Prototyping, and Direct Digital Manufacturing*, Gibson, I.; Rosen, D.; Stucker, B., Eds. Springer New York: New York, NY, **2015**, pp 293-301.
2. Belaid, H.; Nagarajan, S.; Barou, C.; Huon, V.; Bares, J.; Balme, S.; Miele, P.; Cornu, D.; Cavaillès, V.; Teyssier, C.; Bechelany, M., Boron Nitride Based Nanobiocomposites: Design by 3D Printing for Bone Tissue Engineering. *ACS Applied Bio Materials* **2020**.
3. Temple, J. P.; Hutton, D. L.; Hung, B. P.; Huri, P. Y.; Cook, C. A.; Kondragunta, R.; Jia, X.; Grayson, W. L., Engineering anatomically shaped vascularized bone grafts with hASCs and 3D-printed PCL scaffolds. *Journal of Biomedical Materials Research Part A* **2014,** *102* (12), 4317-4325.
4. Belaid, H.; Nagarajan, S.; Teyssier, C.; Barou, C.; Barés, J.; Balme, S.; Garay, H.; Huon, V.; Cornu, D.; Cavaillès, V.; Bechelany, M., Development of new biocompatible 3D printed graphene oxide-based scaffolds. *Materials Science and Engineering: C* **2020,** *110*, 110595.
5. He, H.-Y.; Zhang, J.-Y.; Mi, X.; Hu, Y.; Gu, X.-Y., Rapid prototyping for tissue-engineered bone scaffold by 3D printing and biocompatibility study. *Int J Clin Exp Med* **2015,** *8* (7), 11777-11785.
6. Sun, H.; Mei, L.; Song, C.; Cui, X.; Wang, P., The in vivo degradation, absorption and excretion of PCL-based implant. *Biomaterials* **2006,** *27* (9), 1735-1740.
7. Más Estellés, J.; Vidaurre, A.; Meseguer Dueñas, J. M.; Castilla Cortázar, I., Physical characterization of polycaprolactone scaffolds. *Journal of Materials Science: Materials in Medicine* **2008,** *19* (1), 189-195.
8. Matzinos, P.; Tserki, V.; Gianikouris, C.; Pavlidou, E.; Panayiotou, C., Processing and characterization of LDPE/starch/PCL blends. *European Polymer Journal* **2002,** *38* (9), 1713-1720.
9. Osteogenic Induction of Human Bone Marrow-Derived Mesenchymal Progenitor Cells in Novel Synthetic Polymer–Hydrogel Matrices. *Tissue Engineering* **2003,** *9* (4), 689-702.
10. Darouiche, R. O., Treatment of Infections Associated with Surgical Implants. *New England Journal of Medicine* **2004,** *350* (14), 1422-1429.
11. Trampuz, A.; Widmer, A. F., Infections associated with orthopedic implants. *Current Opinion in Infectious Diseases* **2006,** *19* (4), 349-356.
12. Lazzarini, L.; Mader, J. T.; Calhoun, J. H., Osteomyelitis in Long Bones. *JBJS* **2004,** *86* (10), 2305-2318.
13. Lew, D. P.; Waldvogel, F. A., Osteomyelitis. *The Lancet* **2004,** *364* (9431), 369-379.
14. Visscher, L. E.; Dang, H. P.; Knackstedt, M. A.; Hutmacher, D. W.; Tran, P. A., 3D printed Polycaprolactone scaffolds with dual macro-microporosity for applications in local delivery of antibiotics. *Materials Science and Engineering: C* **2018,** *87*, 78-89.
15. Morones-Ramirez, J. R.; Winkler, J. A.; Spina, C. S.; Collins, J. J., Silver enhances antibiotic activity against gram-negative bacteria. *Sci Transl Med* **2013,** *5* (190), 190ra81-190ra81.
16. Lu, S.; Yu, J.; Cheng, Y.; Wang, Q.; Barras, A.; Xu, W.; Szunerits, S.; Cornu, D.; Boukherroub, R., Preparation of silver nanoparticles/polydopamine functionalized polyacrylonitrile fiber paper and its catalytic activity for the reduction 4-nitrophenol. *Applied Surface Science* **2017,** *411*, 163-169.
17. Patil, D. S.; Pawar, S. A.; Patil, P. S.; Kim, J. H.; Shin, J. C., Silver Nanoparticles Incorporated PEDOT-PSS Electrodes for Electrochemical Supercapacitor. *Journal of Nanoscience and Nanotechnology* **2016,** *16* (10), 10625-10629.
18. Lee, T.-W.; Lee, S.-E.; Jeong, Y. G., Highly Effective Electromagnetic Interference Shielding Materials based on Silver Nanowire/Cellulose Papers. *ACS Applied Materials & Interfaces* **2016,** *8* (20), 13123-13132.
19. Choudhury, A., Polyaniline/silver nanocomposites: Dielectric properties and ethanol vapour sensitivity. *Sensors and Actuators B: Chemical* **2009,** *138* (1), 318-325.

20. Qing, Y. a.; Cheng, L.; Li, R.; Liu, G.; Zhang, Y.; Tang, X.; Wang, J.; Liu, H.; Qin, Y., Potential antibacterial mechanism of silver nanoparticles and the optimization of orthopedic implants by advanced modification technologies. *Int J Nanomedicine* **2018,** *13*, 3311-3327.
21. Correia, T. R.; Figueira, D. R.; de Sá, K. D.; Miguel, S. P.; Fradique, R. G.; Mendonça, A. G.; Correia, I. J., 3D Printed scaffolds with bactericidal activity aimed for bone tissue regeneration. *International Journal of Biological Macromolecules* **2016,** *93*, 1432-1445.
22. Vasilev, K.; Cook, J.; Griesser, H. J., Antibacterial surfaces for biomedical devices. *Expert Review of Medical Devices* **2009,** *6* (5), 553-567.
23. Muwaffak, Z.; Goyanes, A.; Clark, V.; Basit, A. W.; Hilton, S. T.; Gaisford, S., Patient-specific 3D scanned and 3D printed antimicrobial polycaprolactone wound dressings. *International Journal of Pharmaceutics* **2017,** *527* (1), 161-170.
24. Deng, L.; Deng, Y.; Xie, K., AgNPs-decorated 3D printed PEEK implant for infection control and bone repair. *Colloids and Surfaces B: Biointerfaces* **2017,** *160*, 483-492.
25. Zhang, Y.; Zhai, D.; Xu, M.; Yao, Q.; Zhu, H.; Chang, J.; Wu, C., 3D-printed bioceramic scaffolds with antibacterial and osteogenic activity. *Biofabrication* **2017,** *9* (2), 025037.
26. Silver Nanoparticle Impregnated Poly (ε-Caprolactone) Scaffolds: Optimization of Antimicrobial and Noncytotoxic Concentrations. *Tissue Engineering Part A* **2011,** *17* (3-4), 439-449.
27. Kalakonda, P.; Aldhahri, M. A.; Abdel-wahab, M. S.; Tamayol, A.; Moghaddam, K. M.; Ben Rached, F.; Pain, A.; Khademhosseini, A.; Memic, A.; Chaieb, S., Microfibrous silver-coated polymeric scaffolds with tunable mechanical properties. *RSC Advances* **2017,** *7* (55), 34331-34338.
28. Zhou, Y.; Thakurathi, M.; Quitevis, E. L.; Tan, G. Z., Electrospinning 3D Nanofiber Structure of Polycaprolactone Incorporated with Silver Nanoparticles. *JOM* **2019,** *71* (3), 956-962.
29. Vu, T.-L.; Barés, J., Soft-grain compression: Beyond the jamming point. *Physical Review E* **2019,** *100* (4), 042907.
30. Vu, T. L.; Barés, J.; Mora, S.; Nezamabadi, S., Deformation Field in Diametrically Loaded Soft Cylinders. *Experimental Mechanics* **2019,** *59* (4), 453-467.
31. Pastoriza-Santos, I.; Liz-Marzán, L. M., N,N-Dimethylformamide as a Reaction Medium for Metal Nanoparticle Synthesis. *Advanced Functional Materials* **2009,** *19* (5), 679-688.
32. Park, J.; Lee, S. J.; Jo, H. H.; Lee, J. H.; Kim, W. D.; Lee, J. Y.; Park, S. A., Fabrication and characterization of 3D-printed bone-like β-tricalcium phosphate/polycaprolactone scaffolds for dental tissue engineering. *Journal of Industrial and Engineering Chemistry* **2017,** *46*, 175-181.
33. Murphy, C. M.; Haugh, M. G.; O'Brien, F. J., The effect of mean pore size on cell attachment, proliferation and migration in collagen–glycosaminoglycan scaffolds for bone tissue engineering. *Biomaterials* **2010,** *31* (3), 461-466.
34. Elzein, T.; Nasser-Eddine, M.; Delaite, C.; Bistac, S.; Dumas, P., FTIR study of polycaprolactone chain organization at interfaces. *Journal of Colloid and Interface Science* **2004,** *273* (2), 381-387.
35. López-Esparza, J.; Espinosa-Cristóbal, L. F.; Donohue-Cornejo, A.; Reyes-López, S. Y., Antimicrobial Activity of Silver Nanoparticles in Polycaprolactone Nanofibers against Gram-Positive and Gram-Negative Bacteria. *Industrial & Engineering Chemistry Research* **2016,** *55* (49), 12532-12538.
36. Thomas, S.; Nair, S. K.; Jamal, E. M. A.; Al-Harthi, S. H.; Varma, M. R.; Anantharaman, M. R., Size-dependent surface plasmon resonance in silver silica nanocomposites. *Nanotechnology* **2008,** *19* (7), 075710.
37. Ren, S.; Dong, L.; Zhang, X.; Lei, T.; Ehrenhauser, F.; Song, K.; Li, M.; Sun, X.; Wu, Q., Electrospun Nanofibers Made of Silver Nanoparticles, Cellulose Nanocrystals, and Polyacrylonitrile as Substrates for Surface-Enhanced Raman Scattering. *Materials* **2017,** *10* (1), 68.
38. Pastoriza-Santos, I.; Liz-Marzán, L. M., Formation and Stabilization of Silver Nanoparticles through Reduction by N,N-Dimethylformamide. *Langmuir* **1999,** *15* (4), 948-951.

39. Lv, Q.; Wu, D.; Xie, H.; Peng, S.; Chen, Y.; Xu, C., Crystallization of poly(ε-caprolactone) in its immiscible blend with polylactide: insight into the role of annealing histories. *RSC Advances* **2016,** *6* (44), 37721-37730.
40. Eshraghi, S.; Das, S., Mechanical and microstructural properties of polycaprolactone scaffolds with one-dimensional, two-dimensional, and three-dimensional orthogonally oriented porous architectures produced by selective laser sintering. *Acta Biomaterialia* **2010,** *6* (7), 2467-2476.
41. Ahn, S. H.; Kim, S. H.; Kim, B. C.; Shim, K. B.; Cho, B. G., Mechanical properties of silica nanoparticle reinforced poly(ethylene 2, 6-naphthalate). *Macromolecular Research* **2004,** *12* (3), 293-302.
42. Guerrica-Echevarría, G.; Eguiazábal, J. I.; Nazábal, J., Influence of molding conditions and talc content on the properties of polypropylene composites. *European Polymer Journal* **1998,** *34* (8), 1213-1219.
43. The Design of Scaffolds for Use in Tissue Engineering. Part I. Traditional Factors. *Tissue Engineering* **2001,** *7* (6), 679-689.
44. Khan, I.; Nagarjuna, R.; Dutta, J. R.; Ganesan, R., Enzyme-Embedded Degradation of Poly(ε-caprolactone) using Lipase-Derived from Probiotic Lactobacillus plantarum. *ACS Omega* **2019,** *4* (2), 2844-2852.
45. Neumann, R.; Neunzehn, J.; Hinueber, C.; Flath, T.; Schulze, F. P.; Wiesmann, H. P., 3D-printed poly-ε-caprolactone-CaCO3-biocomposite-scaffolds for hard tissue regeneration. *Express Polym. Lett.* **2019,** *13*, 2-17.
47. Hadrup, N.; Sharma, A. K.; Loeschner, K., Toxicity of silver ions, metallic silver, and silver nanoparticle materials after in vivo dermal and mucosal surface exposure: A review. *Regulatory Toxicology and Pharmacology* **2018,** *98*, 257-267.
48. Erick Pazos-Ortiz, J. H. R.-R., Efrén Amador Hinojos-Márquez , Juan López-Esparza, Alejandro Donohué-Cornejo, Juan Carlos Cuevas-González , León Francisco Espinosa-Cristóbal , and Simón Yobanny Reyes-López, Dose-Dependent Antimicrobial Activity of Silver Nanoparticles on Polycaprolactone Fibers against Gram-Positive and Gram-Negative Bacteria. *Journal of nanomaterials* **2017,** *2017*, 1-8.